Real-time displacement measurement with large range and high accuracy using sinusoidal phase modulating laser diode interferometer

Guotian He (何国田)[1,3], Xiangzhao Wang (王向朝)[1,3], Aijun Zeng (曾爱军)[2]
Feng Tang (唐 锋)[1], and Bingjie Huang (黄炳杰)[1,3]

[1]*Shanghai Institute of Optics and Fine Mechanics, Chinese Academy of Sciences, Shanghai 201800*
[2]*Shanghai Hengyi Optics & Fine Mechanics Co., Ltd., Shanghai 201800*
[3]*Graduate School of the Chinese Academy of Sciences, Beijing 100039*

Received October 27, 2006

To resolve the conflict of large measurement range and high accuracy in the existing real-time laser diode (LD) interferometers for displacement measurement, a novel real-time LD interferometry for displacement measurement is proposed and its measurement principle is analyzed. By use of a new phase demodulation algorithm and a new phase compensation algorithm of real-time phase unwrapping, the measurement accuracy is improved, and the measurement range is enlarged to a few wavelengths. In experiments, the peak-to-peak amplitude of the speaker vibration was 2361.7 nm, and the repeatability was 2.56 nm. The measurement time was less than 26 μs.

OCIS codes: 120.3180, 220.4840, 230.5750.

Optical heterodyne techniques are used to measure displacements of an object in many systems such as information storage and micro-electro-mechanical systems (MEMSs)[1−3]. Sasaki *et al.* have proposed a sinusoidal phase modulating (SPM) interferometer[4]. The phase modulating required in a SPM interferometer can be more easily performed than that in a heterodyne interferometer. The interferometer has been widely used to measure the surface profile, displacement, vibration, and angle displacement with high accuracy[4−8]. Recently, laser diodes (LDs) have been incorporated into SPM interferometer as light sources and phase modulators. LD is small in size and has some attractive features such as wavelength tunability and high efficiency, thus it is suitable for the SPM interferometer with the advantages of small size, simple modulation, high efficiency, etc.[9−11]. When the displacement is measured using the SPM-LD interferometer[12,13], the measurement range and accuracy are contradictory[9,10]. Several methods have been reported to enlarge the displacement measurement range[14,15], but the range is only enlarged to one wavelength and the measurement accuracy is relatively low. Therefore, it is important to improve properties of the existing interferometer for displacement measurement to meet the measurement request of large range and high accuracy.

In this paper, a novel real-time SPM-LD interferometer for displacement measurement with large range and high accuracy is proposed. The phase signal can be obtained in real time from the interference signal with two real-time phase detection circuits. The real phase is obtained using a phase unwrapping circuit to calculate the displacement. The measurement range is enlarged to a few wavelengths or more, the measurement accuracy is improved too.

Figure 1 shows the schematic diagram of the real-time SPM-LD interferometer for displacement measurement with large measurement range and high accuracy. A LD serves as the light source, a Twyman-Green interferometer is used as the optical system. After collimated by lens L1, the laser beam is split into two beams by a beam splitter (BS). One beam is reflected by mirror M and serves as the reference beam and the other is reflected by the object's surface to be measured and serves as the object beam. The interference is formed by the two beams. The interference signal is detected with a photodiode (PD), and then sent to the two real-time phase detection circuits shown in Fig. 2. The real-time phase detection circuit mainly consists of two amplifiers, a calculator, a filter, and a dividing circuit. The detection signals $P_1(t)$ and $P_2(t)$ can be obtained by the real-time phase detector circuits 1 and 2, respectively. The signals $P_1(t)$ and $P_2(t)$,

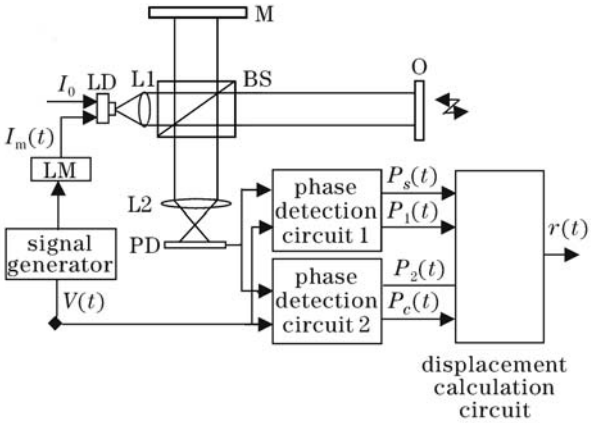

Fig. 1. Schematic diagram of the real-time LD interferometer for displacement measurement with large range and high accuracy.

1671-7694/2007/040211-04

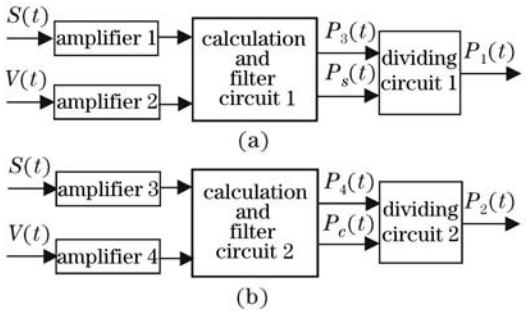

Fig. 2. Two real-time phase detection circuits.

corresponding to different frequencies, are input into a real-time phase unwrapping circuit to obtain the phase. Therefore, the displacement of the measured object can be calculated.

The modulation voltage signal of the LD is generated by a signal generator. It can be transformed into sinusoidal modulation current $I_{\rm m}(t)$ by the LD modulator (LM), and $I_{\rm m}(t)$ is represented by

$$I_{\rm m}(t) = a\cos\omega_0 t, \tag{1}$$

where $a = K_{\rm LM}A$, $K_{\rm LM}$ is the conversion efficiency of the LM, and A is the amplitude of the modulation voltage signal. The injection current of the LD consists of modulation current $I_{\rm m}(t)$ produced by the LM and direct current (DC) I_0. The wavelength change of the LD is $\beta I_{\rm m}(t)$, β is the wavelength modulation coefficient of the LD. Neglecting the noises, the interference signal detected by the PD is given by[16]

$$S(t) = S_1 + S_0\cos[z\cos\omega_0 t + \alpha_0 + \alpha_r(t)], \tag{2}$$

$$z = 4\pi a\beta D_0/\lambda_0^2, \tag{3}$$

$$\alpha_0 = \frac{4\pi}{\lambda_0}D_0, \tag{4}$$

$$\alpha_r(t) = (4\pi/\lambda_0)r(t), \tag{5}$$

where S_1 is the DC component of the interference signal, S_0 is the amplitude of the alternating current (AC) component, z is the SPM depth, λ_0 is the central wavelength of the LD determined by the DC current I_0, α_0 is the initial phase which is determined by the initial optical path difference between the two arms of the interferometer, $\alpha_r(t)$ is the phase change of the interference signal arising from the displacement $r(t)$.

Expanding Eq. (2) and neglecting the DC component, we have[16]

$$S(t) = S_0\{\cos\alpha(t)[J_0(z) - 2J_2(z)\cos 2\omega_0 t + \cdots]$$

$$-\sin\alpha(t)[2J_1(z)\cos\omega_0 t - 2J_3(z)\cos 3\omega_0 t + \cdots]\}, \tag{6}$$

where $\alpha(t) = \alpha_0 + \alpha_r(t)$, $J_n(z)$ is the nth order Bessel function. In the real-time phase detection circuit 1 shown in Fig. 2(a), the interference signal and the modulation signal are amplified by amplifiers 1 and 2, respectively. The two amplified signals are multiply operated by the calculation and filter circuit 1. Subsequently, after filtered by the low-pass filter (LPF), the signal $P_s(t)$ is obtained. The gains of the amplifiers 1 and 2 are K_{1s} and K_{2s}, respectively. The coefficient of the calculation circuit is K_{cs}, and the gain of the filter is K_{ls}, and the cut-off frequency is less than $\omega_0/10$. Therefore, the signal $P_s(t)$ is given by

$$P_s(t) = K_{1s}K_{2s}K_{cs}K_{ls}S_0AJ_1(z)\sin\alpha(t) = K_s\sin\alpha(t), \tag{7}$$

where $K_s = K_{1s}K_{2s}K_{cs}K_{ls}S_0AJ_1(z)$.

After the signal $P_s(t)$ is squared and filtered, the root is extracted, $P_3(t)$ is obtained as

$$P_3(t) = K_s. \tag{8}$$

With the division operation between the signal $P_3(t)$ and $P_s(t)$ by the dividing circuit 1, the detection signal $P_1(t)$ is given by

$$P_1(t) = \sin\alpha(t). \tag{9}$$

In the same way, a signal $P_c(t)$ is obtained with the real-time phase detection circuit 2 shown in Fig. 2(b), given by

$$P_c(t) = K_{1c}K_{2c}K_{cc}K_{lc}S_0AJ_2(z)cos\alpha(t) = K_c\cos\alpha(t), \tag{10}$$

where $K_c = K_{1c}K_{2c}K_{cc}K_{lc}S_0AJ_2(z)$. Correspondingly, K_{1c} and K_{2c} are the gains of the amplifiers 3 and 4, respectively, K_{cc} is the coefficient of the calculation circuit, and K_{lc} is the gain of the low-pass filter. The detection signal $P_2(t)$ is then given by

$$P_2(t) = \cos\alpha(t). \tag{11}$$

Figure 3 shows the block diagram of the displacement calculation circuit, which consists of a dividing circuit, an arctan circuit, a real-time phase unwrapping circuit, and a calculation circuit. The two detection signals $P_s(t)$ and $P_c(t)$ are led to the circuit. Using the dividing circuit and the arctan circuit, the phase is obtained as

$$\alpha(t) = \arctan[P_s(t)/P_c(t)]. \tag{12}$$

According to the phase processed by the calculation circuit, the displacement of an object is obtained by

$$r(t) = \frac{4\pi}{\lambda_0}\alpha(t). \tag{13}$$

The displacement is independent of the change of light intensity, the initial optical path difference, the amplification coefficient of the circuit, the modulation depth, and the Bessel function. Compared with the method in Ref. [7], the displacement measurement accuracy is enhanced.

If just using Eq. (12) to obtain the phase, the measurement range of the phase $\alpha(t)$ is from $-\pi/2$ to $\pi/2$. Therefore, the maximum measurement range of $r(t)$ is $\lambda/2$. To enlarge the measurement range, the phase unwrapping technique is used. When the displacement exceeds the maximum measurement range of $\lambda/2$,

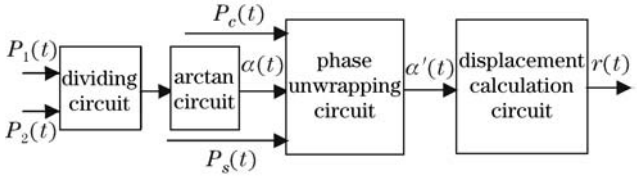

Fig. 3. Block diagram of the displacement calculation circuit.

Table 1. Phase Compensation

$\sin\alpha(t)$	$\cos\alpha(t)$	4-1 Selector	Phase Compensate $\Delta\alpha$	Real Phase α'	Range of α
1	1	1	0	α	$0-\pi/2$
1	0	1	π	$\pi+\alpha$	$-\pi/2-0$
0	0	1	π	$\pi+\alpha$	$0-\pi/2$
0	1	1	0	$2\pi+\alpha$	$-\pi/2-0$

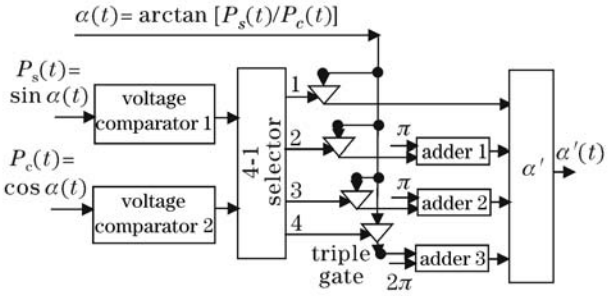

Fig. 4. Block diagram of the real-time phase unwrapping circuit.

the phases are discontinuous. By detecting the change of the values of $\sin\alpha(t)$ and $\cos\alpha(t)$, we can compensate the phase of interference signal to enlarge the measurement range. The phase compensation principle is shown in Table 1. In this way, the measurement range can be more than one wavelength. For real-time measurements, the phase unwrapping can be completed by the real-time phase unwrapping circuit shown in Fig. 4.

In Table 1, when the value of $\sin\alpha(t)$ or $\cos\alpha(t)$ is plus, we express it as 1, and when the value of $\sin\alpha(t)$ or $\cos\alpha(t)$ is minus, we express it as 0. The 4-1 selector has four output paths, only one path works in the same time. In Fig. 4, the value of $\sin\alpha(t)$ or $\cos\alpha(t)$ as 0 or 1 is obtained using the voltage comparator.

The real phase $\alpha'(t)$ is obtained using the 4-1 selector and adder circuit, and $\alpha'(t) = \Delta\alpha + \alpha$. Only one of the 4-1 selector circuit output paths works in the same time, for example, only the 2th path when $\sin\alpha(t) = 1$ and $\cos\alpha(t) = 0$. The displacement of the object is obtained by the displacement calculation circuit, $r(t) = \frac{4\pi}{\lambda_0}\alpha'(t)$.

Delay time of signal processing is mostly dependent on the filtering time and calculation circuit running time of the real-time phase unwrapping circuit. The total delay time of this signal processing system is about 26 μs.

The phase unwrapping mainly includes two types, one is Fourier transform method which is a non-real-time displacement measurement technique[5], the other is a real-time one by synchronous sampling of the sinusoidal phase modulated interference signal[6]. The time delay of the signal processing of the non-real-time one is relatively long.

The experiment was performed using the setup shown in Fig. 1. The LD's maximum output power was 10 mW. The central operating wavelength λ_0 was 785 nm. The wavelength modulation coefficient β was 1.56×10^{-3} nm/mA. The frequency of the SPM signal was 20 kHz. The gains of amplifiers 1 and 2 were 78.2 and 86.9, respectively. The conversion fraction of LM was 0.02 mA/mV and the coefficient of the calculation circuit was 5×10^{-5} mV^{-1}. We chose a 3rd order LPF with the cut-off frequency of 300 Hz, the gain of LPF was 8. The object to be measured was a mirror attached to a speaker, which was driven by a sinusoidal signal. The interference signal was detected by a PD, and transformed into electric signal. The electric signal was processed by the two real-time phase detector circuits and the real-time phase unwrapping circuit to obtain the displacement, the result was displayed by an oscilloscope.

In the experiments, the sinusoidal signal from the signal generator with the frequency of 200 Hz drived the speaker to vibrate sinusoidally along the optical axis. When the frequency of the SPM signal ω_0 was 20 kHz, we adjusted the voltage of the sinusoidal signal and the optical path difference to guarantee the modulation depth 2.35 rad. Figure 5(a) shows the measurement result, the peak-to-peak amplitude ($V_{\mathrm{p-p}}$) of the curve is 2361.7 nm and the frequency is 100 Hz. Figure 5(b) shows another measurement result. The time interval between the two measurements was a few minutes. The repeatability derived from multiple measurements was 2.56 nm. The measurement range is 6 times of that in Ref. [13] with a better repeatability.

The measured displacement with the frequency of the sinusoidally driven signal of 200 Hz is shown in Fig. 6(a). The $V_{\mathrm{p-p}}$ value of the measured curve is 1163.8 nm, and the frequency is 100 Hz. Figure 6(b) shows another result. The repeatability derived from multiple measurements is 2.92 nm.

For comparison, we measured the displacement using the photothermal modulated SPM-LD interferometer[10]. The frequency of the sinusoidal voltage signal on the

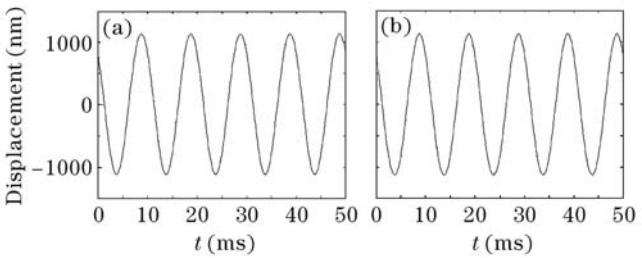

Fig. 5. Measured displacement-time curves with 100-Hz frequency.

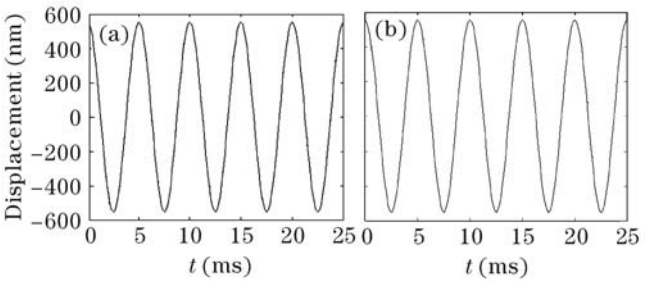

Fig. 6. Measured displacement-time curves with 200-Hz frequency.

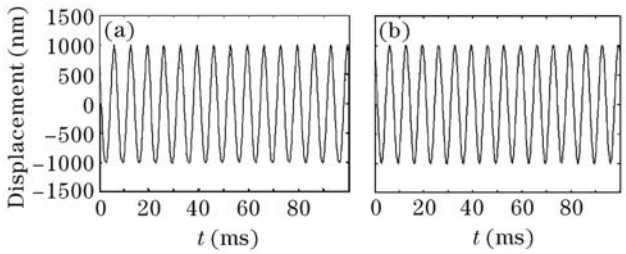

Fig. 7. Measurement results with (a) the photo-thermal LD SPM interferometer and (b) the interferometer shown in Fig. 1.

speaker was 150 Hz and the vibration amplitude of the vibrating mirror attached to the speaker was 1008 nm. In the photothermal modulated LD SPM interferometer, electric signal output from the PD was amplified by an amplification circuit and input into a computer by the acquisition card. With the discrete Fourier transformation[10] and the algorithm for enlarged measurement range, the displacement of the speaker was obtained. The result is shown in Fig. 7(a). The amplitude of the curve is 1010.16 nm and the frequency is 150 Hz. The root-mean-square (RMS) error is 1.52 nm after multiple measurements. One of the LDs of the photothermal modulated LD SPM interferometer was removed to form the optical system shown in Fig. 1. The two real-time phase detection circuits and the real-time phase unwrapping circuit were used to process the interference signal. Figure 7(b) shows the displacement measurement result. In this curve, $V_{\mathrm{p-p}}$ is 1011.98 nm and frequency is 150 Hz. The RMS error between the two measurements is 3.16 nm. The measurement range was not enlarged further because of the limits of experimental conditions.

In this paper, a novel real-time LD interferometer for displacement measurement with high accuracy and large range is proposed. The displacement can be measured with two real-time phase detection circuits and a real-time phase unwrapping circuit. The measurement range is enlarged to a few or more wavelengths. By use of a novel disturbance elimination technique, the measurement result is independent of the fluctuation of light intensity, initial optical path difference, amplification coefficient of the circuit, modulation depth, Bessel function, and the measurement accuracy is improved. In experiments, the displacement measurement range was 2361.7 nm and the repeatability was 2.56 nm, the measurement time was less than 26 μs. The improvement in measurement accuracy and range of the interferometer is verified.

This work was supported by the National Natural Science Foundation of China (No. 60578051) and the Science and Technology Committee of Shanghai (No. 051107085 and 06QB14047). G. He's e-mail address is slhgt@siom.ac.cn.

References

1. R. Shinozaki, O. Sasaki, and T. Suzuki, Appl. Opt. **43,** 4157 (2004).
2. J. D. Zook, W. R. Herb, C. J. Bassett, T. Stark, J. N. Schoess, and M. L. Wilson, Sensors and Actuators A **83,** 270 (2000).
3. S. Venkatesh and B. Culshaw, Electron. Lett. **21,** 315 (1985).
4. O. Sasaki and H. Okazaki, Appl. Opt. **25,** 3137 (1986).
5. O. Sasaki, K. Takahashi, and T. Suzuki, Opt. Eng. **29,** 1511 (1990).
6. T. Suzuki, O. Sasaki, K. Higuchi, and T. Maruyama, Appl. Opt. **28,** 5270 (1989).
7. S. Song, X. Wang, X. Wang, F. Qian, and H. Lu, Acta Opt. Sin. (in Chinese) **21,** 578 (2001).
8. T. Suzuki, H. Nakamura, O. Sasaki, and J. E. Greivenkamp, Opt. Eng. **40,** 426 (2001).
9. T. Suzuki, O. Sasaki, and T. Maruyama, Opt. Eng. **35,** 492 (1996).
10. X. Wang, X. Wang, F. Qian, G. Chen, G. Chen, and Z. Fang, Opt. Laser Technol. **31,** 559 (1999).
11. P. de Groot, Appl. Opt. **30,** 3612 (1991).
12. O. Sasaki, H. Sasazaki, and T. Suzuki, Appl. Opt. **30,** 4040 (1991).
13. O. Sasaki, T. Yoshida, and T. Suzuki, Appl. Opt. **30,** 3617 (1991).
14. T. Suzuki, O. Sasaki, S. Takayama, and T. Maruyama, Opt. Eng. **32,** 1033 (1993).
15. T. Susuki, T. Okada, O. Sasaki, and T. Maruyama, Opt. Eng. **36,** 2496 (1997).
16. S. Song, X. Wang, X. Wang, F. Qin, and G. Chen, Chin. J. Lasers (in Chinese) **28,** 753 (2001).